

Wave-Number-Dependent Gilbert Damping in Metallic Ferromagnets

Y. Li and W. E. Bailey*

*Materials Science and Engineering, Department of Applied Physics and Applied Mathematics,
Columbia University, New York, New York 10027, USA*

(Received 31 October 2013; revised manuscript received 24 January 2016; published 18 March 2016)

A wave-number-dependent dissipative term to magnetization dynamics, mirroring the conservative term associated with exchange, has been proposed recently for ferromagnetic metals. We present measurements of wave-number- (k) -dependent Gilbert damping in three metallic ferromagnets, NiFe, Co, and CoFeB, using perpendicular spin wave resonance up to 26 GHz. In the thinnest films accessible, where classical eddy-current damping is negligible, size effects of Gilbert damping for the lowest and first excited modes support the existence of a k^2 term. The new term is clearly separable from interfacial damping typically attributed to spin pumping. Higher-order modes in thicker films do not show evidence of enhanced damping, attributed to a complicating role of conductivity and inhomogeneous broadening. Our extracted magnitude of the k^2 term, $\Delta\alpha_{kE}^* = \Delta\alpha_0^* + A_k^*k^2$, where $A_k^* = 0.08$ – 0.1 nm² in the three materials, is an order of magnitude lower than that identified in prior experiments on patterned elements.

DOI: 10.1103/PhysRevLett.116.117602

The dynamical behavior of magnetization for ferromagnets (FMs) can be described by the Landau-Lifshitz-Gilbert (LLG) equation [1]:

$$\dot{\mathbf{m}} = -\mu_0|\gamma|\mathbf{m} \times \mathbf{H}_{\text{eff}} + \alpha\mathbf{m} \times \dot{\mathbf{m}}, \quad (1)$$

where μ_0 is the vacuum permeability, $\mathbf{m} = \mathbf{M}/M_s$ is the reduced magnetization unit vector, \mathbf{H}_{eff} is the effective magnetic field, γ is the gyromagnetic ratio, and α is the Gilbert damping parameter. The LLG equation can be equivalently formulated, for small-angle motion, in terms of a single complex effective field along the equilibrium direction, as $\mu_0\dot{H}_{\text{eff}} = \mu_0H_{\text{eff}} - i\alpha\omega/|\gamma|$; damping torque is included in the imaginary part of \dot{H}_{eff} .

For all novel spin-transport related terms to the LLG identified so far [2–7], each real (conservative) effective field term is mirrored by an imaginary (dissipative) counterpart. In spin-transfer torque, there exist both conventional [2,3] and fieldlike [8] terms in the dynamics. In spin-orbit torques (spin Hall [4] and Rashba [6] effect) dampinglike and fieldlike components have been theoretically predicted [9] and most terms have been experimentally identified [5,6]. For pumped spin current [7], theory predicts real and imaginary spin mixing conductances [10] $g_r^{\uparrow\downarrow}$ and $g_i^{\uparrow\downarrow}$, which introduce imaginary and real effective fields, respectively.

It is well known that the exchange interaction, responsible for ferromagnetism, contributes a real effective field (fieldlike torque) quadratic in wave number k for spin waves [11]. It is then natural to ask whether a corresponding imaginary effective field might exist, contributing a dampinglike torque to spin waves. Theoretically, such an interaction has been predicted due to the *intralayer* spin-current transport in a spin wave [12–15], reflected as an additional term in Eq. (1):

$$\dot{\mathbf{m}} = \dots - (|\gamma|\sigma_{\perp}/M_s)\mathbf{m} \times \nabla^2\dot{\mathbf{m}}, \quad (2)$$

where σ_{\perp} is the transverse spin conductivity. This term represents a continuum analog of the well-established interlayer spin pumping effect [7,16,17]. For spin wave resonance (SWR) with well-defined wave number k , Eq. (2) generates an additional Gilbert damping $\Delta\alpha(k) = (|\gamma|\sigma_{\perp}/M_s)k^2$. In this context, Gilbert damping refers to an intrinsic relaxation mechanism through which the field-swept resonance linewidth is proportional to frequency. Remarkably, the possible existence of such a term has not been addressed in prior SWR measurements. Previous studies of ferromagnetic resonance (FMR) linewidths of spin waves [18–21] were typically operated at fixed frequency, not allowing separation of intrinsic (Gilbert) and extrinsic linewidths. Experiments have been carried out on thick FM films, susceptible to a large eddy-current damping contribution [22]. Any wave-number-dependent linewidth broadening in these systems has been attributed to eddy currents or inhomogeneous broadening, not intrinsic torques which appear in the LLG equation.

In this Letter, we present a study of wave-number-dependent Gilbert damping in the commonly applied ferromagnetic films Ni₇₉Fe₂₁ (Py), Co, and Co₄₀Fe₄₀B₂₀ (CoFeB). A broad range of film thicknesses (25–200 nm) has been studied in order to exclude eddy-current effects. We observe a thickness-dependent difference in the Gilbert damping for uniform and first excited spin wave modes, which is explained well by the intralayer spin pumping model [14]. Corrections for interfacial damping, or conventional spin pumping, have been applied and are found to be small. The measurements show that the wave-number-dependent damping, as identified in continuous films, is in reasonable agreement with the transverse

spin relaxation lengths measured in Ref. [23], but an order of magnitude smaller than identified in experiments on submicron patterned Py elements [24].

Two different types of thin-film heterostructures were investigated in this study. Films were deposited by UHV sputtering with conditions given in Refs. [23,25]. Multilayers with the structure Si/SiO₂(substrate)/Ta(5nm)/Cu(5nm)/M(*t_M*)/Cu(5nm)/Ta(5nm), where *M* = Py, Co, and CoFeB and *t_M* = 25–200 nm, were designed to separate the effects of eddy-current damping and the intralayer damping mechanism proposed in Eq. (2). The minimum thickness investigated here is our detection threshold for the first SWR mode, 25 nm. A second type of heterostructure focused on much thinner Py films, with the structure Si/SiO₂(substrate)/Ta(5 nm)/Cu(5 nm)/Py(*t_{Py}*)/Cu(5 nm)/X(5 nm), *t_{Py}* = 3–30 nm. Here the cap layer *X* = Ta or SiO₂ was changed, for two series of this type, in order to isolate the effect of interfacial damping (spin pumping) from Cu/Ta interfaces.

To study the Gilbert damping behavior of finite-wave number spin waves in the samples, we have excited perpendicular standing spin wave resonance (PSSWR) [26] using a coplanar waveguide from 3 to 26 GHz. The spin-wave mode dispersion is given by the Kittel equation $\omega(k)/|\gamma| = \mu_0[H_{\text{res}} - M_s + H_{\text{ex}}(k)]$; the effective field from exchange, $\mu_0 H_{\text{ex}}(k) = (2A_{\text{ex}}/M_s)k^2$ with *A_{ex}* as the exchange stiffness, gives a precise measurement of the wave number excited (Fig. 1, inset). PSSWR modes are indexed by the number of nodes *p*, with $k = p\pi/t_M$ in the limit of unpinned surface spins. The full-width half-maximum linewidth, $\Delta H_{1/2}$, is fitted using $\mu_0 \Delta H_{1/2}(\omega) =$

$\mu_0 \Delta H_0 + 2\alpha\omega/|\gamma|$ to extract the Gilbert damping α . For *p* = 1 modes we fix $\mu_0 \Delta H_0$ as the values extracted from the corresponding *p* = 0 modes for (*t_M* ≤ 40 nm), because frequency ranges are reduced due to large exchange fields. In unconstrained fits for films of this thickness, the inhomogeneous broadening $\mu_0 \Delta H_0$ of the *p* = 1 modes does not exhibit a discernible trend with $1/t_M^2$ (or k^2) [19–21], justifying this approximation [27].

To fit our data, we have solved Maxwell's equations and the LLG equation [Eq. (1)], including novel torques such as those given in Eq. (2), according to the method of Rado [34]. The model (designated “EM+LLG”) is described in the Supplemental Material [27]. Values calculated using the EM + LLG model are shown with curves in Fig. 1 and dashed lines in Fig. 4. Comparison with such a model has been necessary since in our first type of sample series, *t_M* = 25 – 200 nm, eddy-current damping is negligible for thinner films (25 nm), the *A_k**k*² contribution is negligible for thicker films (200 nm), but the two effects coexist for the intermediate region.

In Figs. 1(a)–1(c) we compare the measured Gilbert damping for the uniform (*p* = 0, α_u) and first excited (*p* = 1, α_s) spin wave modes. The dominant thickness-dependent contribution to Gilbert damping of the uniform modes of Py, Co, and CoFeB is clearly due to eddy currents which are quadratic in thickness. Note that eddy-current damping is negligible for the thinnest films investigated (25 nm), but quite significant for the thickest films (200 nm). This term sums with the bulk Gilbert damping α_0 [35]. The simulation of α_u , shown by black curves in Fig. 1, matches closely with the analytical expression for bulk and eddy-current damping only [36] of $\alpha_u = \alpha_{u0} + \alpha_{E0}$, where $\alpha_{E0} = \mu_0^2 \gamma M_s t_M^2 / 12 \rho_c$ denotes the eddy-current damping for uniform modes. Fits of α_u yield resistivities $\rho_c = 16.7, 26.4,$ and $36.4 \mu\Omega \text{ cm}$ for Py, Co, and CoFeB, respectively.

Unlike the uniform-mode damping, the first SWR mode damping α_s is found to exhibit a minimum as a function of thickness. For decreasing thicknesses below 75 nm, α_s is increased. This behavior indicates an additional source of Gilbert damping for the 1st SWR modes. In CoFeB the increased α_s is less visible in Fig. 1(c) due to fluctuations in damping for samples of different thickness, but is evident in the difference, $\alpha_s - \alpha_u$, plotted in Fig. 2.

In order to isolate this new damping mechanism, we plot in Fig. 2 the increased damping for the 1st SWR mode, $\Delta\alpha_k = \alpha_s - \alpha_u$, side-by-side with exchange field $\mu_0 H_{\text{ex}}$ as a function of $(\pi/t_M)^2$ taken as the wave number k^2 . When π/t_M is large, a linear k^2 dependence of $\Delta\alpha_k$ in all three ferromagnets mirrors the linear dependence of $\mu_0 H_{\text{ex}}$ on k^2 . This parallel behavior reflects the wave-number-dependent imaginary and real effective fields acting on magnetization, respectively. To quantify the quadratic wave number term in $\Delta\alpha_k$, we also show the eddy-current-corrected values $\Delta\alpha_{kE} = \Delta\alpha_k - \Delta\alpha_E$ in Fig. 2(a). Here $\Delta\alpha_E = \alpha_{E1} - \alpha_{E0}$

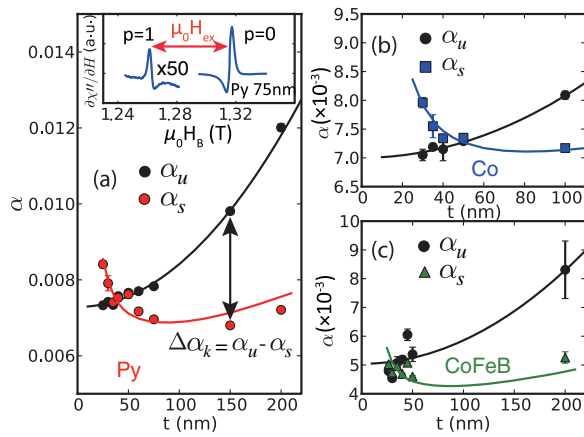


FIG. 1. Thickness dependence of α_u and α_s for (a) Py, (b) Co, and (c) CoFeB thin films. Curves are calculated from a combined solution of Maxwell's equations and the LLG (EM + LLG). For α_u the values of $\mu_0 M_s$, α (Table I), effective spin mixing conductance [27], *g* factor (2.12 for Py and CoFeB and 2.15 for Co), and ρ_c (from analytical fitting) are used. For α_s the values of $\Delta\alpha_{kE}^*$ and $\Delta\alpha_{k0}^*$ (Table I) are also included in the simulation. Inset: 10 GHz FMR spectra of *p* = 0 and *p* = 1 modes in Py 75 nm film.

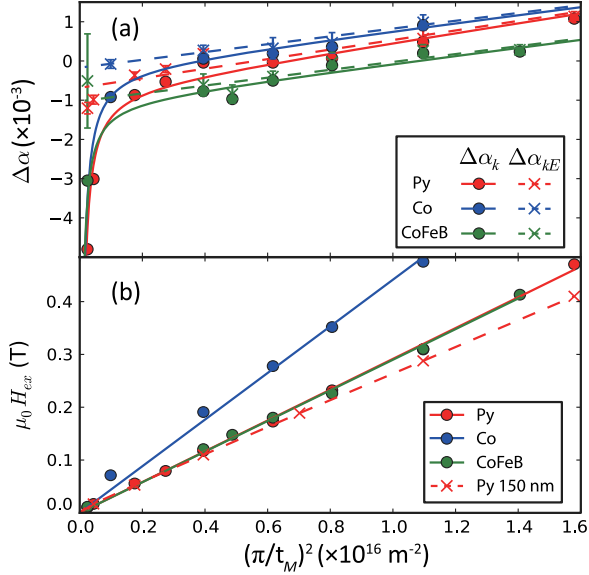


FIG. 2. Imaginary [damping, (a)] and real [exchange, (b)] effective fields as a function of k^2 for Py, Co, and CoFeB. (a) Additional SWR damping $\Delta\alpha_k$ (circle) and eddy-current corrected value $\Delta\alpha_{kE}$ (cross) as a function of $(\pi/t_M)^2$. Solid lines are guides to the eye and dashed lines are fits to Eq. (3). (b) Exchange field $\mu_0 H_{ex}$ as a function of $(\pi/t_M)^2$ [$(p\pi/t_M)^2$, $p = 0 - 6$, for Py 150 nm]. Lines are fits to $\mu_0 H_{ex} = (2A/M_s)k^2$.

denotes the difference in eddy current damping between the $p = 1$ and $p = 0$ modes according to the theory of Ref. [36], for weak surface pinning, where $\alpha_{E1} \approx 0.23\alpha_{E0}$ [27]. We then fit this eddy-current-corrected value to a linearization of Eq. (2), as

$$\Delta\alpha_{kE} = \Delta\alpha_{k0} + A_k k^2, \quad (3)$$

with $A_k = |\gamma|\sigma_{\perp}/M_s$ and $\Delta\alpha_{k0}$ a constant offset. The values of A_k estimated this way are $0.128 \pm 0.022 \text{ nm}^2$, $0.100 \pm 0.011 \text{ nm}^2$, and $0.100 \pm 0.018 \text{ nm}^2$ for Py, Co, and CoFeB.

Recently, Kapelrud *et al.* [37] have predicted that interface-localized (e.g., spin-pumping) damping terms will also be increased in SWR, with interfacial terms for $p \geq 1$ modes a factor of 2 greater than those for the $p = 0$ mode. Using the second series of thinner Py films, we have applied corrections for the interfacial term to our data, and find that these effects introduce only a minor ($\sim 20\%$) correction to the estimate of A_k . The $p = 0$ mode damping associated with the Cu/Ta interface has been measured from the increase in damping upon replacement of SiO_2 with Ta at the top surface (Fig. 3, inset). Here, Cu/ SiO_2 is taken as a reference with zero interfacial damping; insulating layers have been shown to have no spin pumping contribution [38]. We find the damping enhancement to be inversely proportional to t_M , indicating an interfacial damping term quantified as spin pumping into Ta [7] with $\Delta\alpha_{sp} = \gamma\hbar g^{\uparrow\downarrow}/(4\pi M_s t_M)$. Using the values in Table I

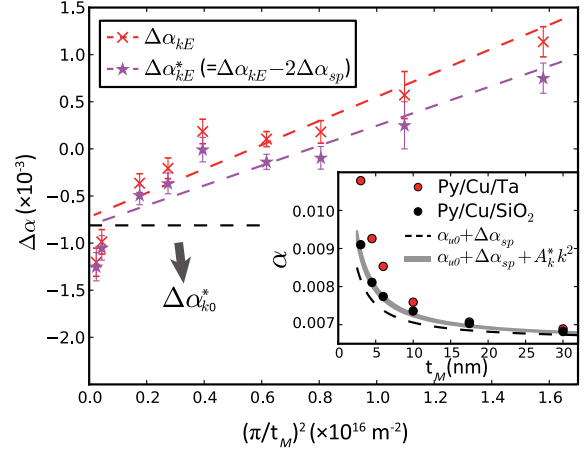


FIG. 3. Wavenumber-dependent damping with ($\Delta\alpha_{kE}$) and without ($\Delta\alpha_{kE}$) the spin pumping-interfacial damping correction. Main panel: $\Delta\alpha_{kE}$ and $\Delta\alpha_{kE}^*$ as a function of $(\pi/t_M)^2$. Dashed lines are fits to k^2 -dependent equation as Eq. (3); $\Delta\alpha_{k0}^*$ are extracted from $\Delta\alpha_{kE}^*$ fits. Inset: size effect of uniform-modes Gilbert damping in Py/Cu/Ta and Py/Cu/ SiO_2 samples (circles). The dashed curve is the theoretical reproduction of Py/Cu/ SiO_2 using $\alpha_{u0} + \Delta\alpha_{sp}(t_M)$. The shadow is the same reproduction using $\alpha_{u0} + \Delta\alpha_{sp}(t_M) + A_k^* k^2$ where the error of shadow is from A_k^* . Here k is determined by $A_{ex} k^2 = 2K_s/t_M$.

yields the effective spin mixing conductance as $g_{\text{Py/Cu/Ta}}^{\uparrow\downarrow} = 2.5 \text{ nm}^{-2}$, roughly a factor of 3 smaller than that contributed by Cu/Pt interfaces [17].

Using the fitted $g_{\text{Py/Cu/Ta}}^{\uparrow\downarrow}$, we calculate and correct for the additional spin pumping contribution to damping of the $p = 1$ mode, $2\Delta\alpha_{sp}$ (from top and bottom interfaces). The corrected values for the 1st SWR damping enhancement, $\Delta\alpha_{kE}^* = \Delta\alpha_{kE} - 2\Delta\alpha_{sp}$, are plotted for Py (25–200 nm) in Fig. 3. These corrections do not change the result significantly. We fit the k^2 dependence of $\Delta\alpha_{kE}^*$ to Eq. (3) to extract the corrected values A_k^* and $\Delta\alpha_{k0}^*$. The fitted value, $A_k^* = 0.105 \pm 0.021 \text{ nm}^2$ for Py, is slightly smaller than the uncorrected value A_k . Other extracted interfacial-corrected values A_k^* are listed in Table I. Note that the correction of wave number by finite surface anisotropy will only introduce a small correction of A_k and A_k^* within error bars. We also show the EM + LLL numerical simulation results for the uniform modes and the first SWR modes in Fig. 1 (solid curves). Those curves coincide with the analytical expressions of eddy-current damping plus k^2 damping (not shown) and fit the experimental data points well for Py, Co, and CoFeB.

The negative offsets $\Delta\alpha_{k0}^*$ between uniform modes and spin wave modes for Py and CoFeB could be attributed to resistivitylike intrinsic damping [39]: because \mathbf{m} is averaged through the whole film for uniform modes and maximized at the interfaces for unpinned boundary condition, the SWR mode experiences a lower resistivity near low-resistivity Cu and thus a reduced value of damping.

TABLE I. Fit parameters extracted from resonance fields and linewidths of uniform and 1st SWR modes. Values of A_k^* and $\Delta\alpha_0^*$ for Co and CoFeB are calculated using the spin mixing conductances measured in FM/Cu/Pt [27].

	$\mu_0 M_s$ (T)	α_0	A_{ex} (J/m)	A_k^* (nm ²)	$\Delta\alpha_0^*$
Py	1.00	0.0073	1.2×10^{-11}	0.11 ± 0.02	-0.0008
Co	1.47	0.0070	3.1×10^{-11}	0.08 ± 0.01	-0.0002
CoFeB	1.53	0.0051	1.8×10^{-11}	0.09 ± 0.02	-0.0011

For Co, a transition state between resistivitylike and conductivitylike mechanisms around room temperature [40] corresponds to negligible $\Delta\alpha_{k0}^*$ as observed in this work.

In addition to the thickness-dependent comparison of $p = 0$ and $p = 1$ modes, we have also measured Gilbert damping for a series of higher-order modes in a thick Py (150 nm) film. Eddy-current damping ($\alpha_E \sim 0.003$) is the dominant mode-dependent contribution in this film. The wave number k for the mode $p = 6$ is roughly equal to that for the first SWR, $p = 1$, in the 25 nm film. Resonance positions are plotted with the dashed lines in Fig. 2(b), as a function of k , and are in good agreement with those found from the $p = 1$ data. In Fig. 4 we plot the mode-related Gilbert damping α_p up to $p = 6$, seen to gradually decrease as p increases. We have again conducted full numerical simulations using the EM + LLG method with ($A_k^* = 0.105$ nm²) or without ($A_k^* = 0$) the intralayer spin pumping term, shown with red and black crosses, respectively. Neither scenario fits the data closely; an increase at $p = 3$ is closer to the model including the k^2 mechanism, but experimental α at $p = 6$ falls well below either calculation.

We believe there are two possibilities why the $\alpha \propto p^2$ damping term is not evident in this configuration. First, the

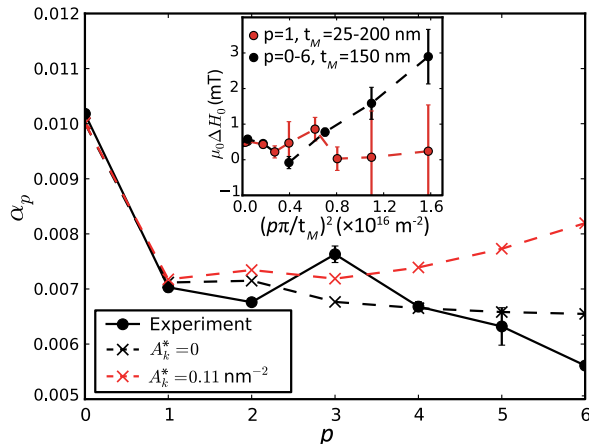


FIG. 4. Mode-dependent damping α_p for Py(150 nm), $0 \leq p \leq 6$. Crosses are EM + LLG calculated values with and without the wave-number-dependent damping term. Inset: Inhomogeneous broadening ΔH_0 vs $0 \leq p \leq 6$, 150 nm film. Larger, k -dependent values are evident, compared with those in the thickness series ($t_M = 25\text{--}200$ nm).

effective exchange field increases with p , resulting in a weaker (perpendicular) resonance field at the same frequency. When the perpendicular biasing field at resonance is close to the saturation field, the spins near the boundary may not be fully saturated, creating inhomogeneous linewidth broadening at lower frequencies and masking small Gilbert contributions from the wavenumber-dependent term. From the data in Fig. 4 inset the high- p SWR modes are more affected by this inhomogeneous broadening. Second, high- p modes in thick films are close to the anomalous conductivity regime, $k\lambda_m \sim 1$, where λ_m is the electronic mean free path. The Rado-type model such as that applied in Fig. 4 is no longer valid in this limit [41], beyond which Gilbert damping has been shown to decrease significantly in Ni and Co [42]. Based on published $\rho\lambda_m$ products for Py [43] and our experimental value of $\rho_c = 16.7$ $\mu\Omega$ cm, we find $\lambda_m \sim 8$ nm and $k\lambda_m \sim 1$ for the $p = 6$ mode in Py 150 nm. For the 1st SWR mode in Py 25 nm, on the other hand, eddy currents are negligible and the anomalous behavior is likely suppressed due to surface scattering, which reduces λ_m .

An important conclusion of our work is that the intralayer spin pumping, as measured classically through PSSWR, is indeed present but roughly 10 times smaller than estimated in single nanoscale ellipses [24]. The advantages of the PSSWR measurements presented in this manuscript are that the one-dimensional mode profile is well defined, two-magnon effects are reduced, if not absent [44], and there are no lithographic edges to complicate the analysis. The lower estimates of A_k^* from PSSWR are sensible, based on the physical parameters of Py, Co, and CoFeB. The polarization of continuum-pumped spins in a nearly uniformly magnetized film, like that of the pumped spin current in a parallel-magnetized ferromagnet-normal-metal-ferromagnet structure, is transverse to the magnetization [14]. From the measured transverse spin conductance σ_{\perp} we extract that the relaxation lengths of pumping intralayer spin current are 0.8–1.9 nm for the three ferromagnets [27], in good agreement with the small transverse spin coherence lengths found in these same ferromagnetic metals [23,45].

Finally, we show that the magnitude of the intralayer spin pumping identified here is consistent with the damping size effect *not* attributable to interlayer spin pumping, in layers without obvious spin sinks. For the $p = 0$ mode, a small but finite wave number is set by the surface anisotropy through [36,46] $A_{\text{ex}}k^2 = 2K_s/t_M$. The damping enhancement due to intralayer spin pumping will, like the interlayer spin pumping, be inverse in thickness, leading to an “interfacial” term as $\alpha = 2K_s(A_k^*/A_{\text{ex}})t_M^{-1}$. This contribution is indicated by the gray shadow in Fig. 3 inset and provides a good account of the additional size effect in the SiO₂-capped film. Here we use $K_s = 0.11$ mJ/m² extracted by fitting the thickness-dependent magnetization to $\mu_0 M_{\text{eff}} = \mu_0 M_s - 4K_s/M_s t_M$. While alternate contributions to the observed damping size

effect for the SiO₂-capped film cannot be ruled out, the data in Fig. 3 inset place an upper bound on A_k^* .

In summary, we have identified a wave-number-dependent, Gilbert-type damping contribution to spin waves in nearly uniformly magnetized, continuous films of the metallic ferromagnets Py, Co, and CoFeB using classical spin wave resonance. The term varies quadratically with wave number $\Delta\alpha \sim A_k^* k^2$, with the magnitude $A_k^* \sim 0.08\text{--}0.10\text{ nm}^2$, amounting to $\sim 20\%$ of the bulk damping in the first excited mode of a 25 nm film of Py or Co, roughly an order of magnitude smaller than previously identified in patterned elements. The measurements quantify this texture-related contribution to magnetization dynamics in the limit of nearly uniform magnetization.

We acknowledge support from the National Science Foundation, Grants No. NSF-ECCS-0925829 and No. NSF-DMR-1411160.

*Corresponding author.
web54@columbia.edu

- [1] T. L. Gilbert, *IEEE Trans. Magn.* **40**, 3443 (2004).
 [2] J. C. Slonczewski, *J. Magn. Magn. Mater.* **159**, L1 (1996).
 [3] L. Berger, *Phys. Rev. B* **54**, 9353 (1996).
 [4] J. E. Hirsch, *Phys. Rev. Lett.* **83**, 1834 (1999).
 [5] S. O. Valenzuela and M. Tinkham, *Nature (London)* **442**, 176 (2006).
 [6] I. M. Miron, G. Gaudin, S. Auffret, B. Rodmacq, A. Schuhl, S. Pizzini, J. Vogel, and P. Gambardella, *Nat. Mater.* **9**, 230 (2010).
 [7] Y. Tserkovnyak, A. Brataas, and G. E. W. Bauer, *Phys. Rev. Lett.* **88**, 117601 (2002).
 [8] S. Zhang, P. M. Levy, and A. Fert, *Phys. Rev. Lett.* **88**, 236601 (2002).
 [9] P. M. Haney, H. W. Lee, K. J. Lee, A. Manchon, and M. D. Stiles, *Phys. Rev. B* **87**, 174411 (2013).
 [10] M. Zwierzycki, Y. Tserkovnyak, P. J. Kelly, A. Brataas, and G. E. W. Bauer, *Phys. Rev. B* **71**, 064420 (2005).
 [11] C. Kittel, *Phys. Rev.* **81**, 869 (1951).
 [12] E. M. Hankiewicz, G. Vignale, and Y. Tserkovnyak, *Phys. Rev. B* **78**, 020404(R) (2008).
 [13] J. Foros, A. Brataas, Y. Tserkovnyak, and G. E. W. Bauer, *Phys. Rev. B* **78**, 140402(R) (2008).
 [14] Y. Tserkovnyak, E. M. Hankiewicz, and G. Vignale, *Phys. Rev. B* **79**, 094415 (2009).
 [15] S. Zhang and S. S.-L. Zhang, *Phys. Rev. Lett.* **102**, 086601 (2009).
 [16] S. Mizukami, Y. Ando, and T. Miyazaki, *Phys. Rev. B* **66**, 104413 (2002).
 [17] A. Ghosh, J. F. Sierra, S. Auffret, U. Ebels, and W. E. Bailey, *Appl. Phys. Lett.* **98**, 052508 (2011).
 [18] P. E. Wigen, *Phys. Rev.* **133**, A1557 (1964).
 [19] T. G. Phillips and H. M. Rosenberg, *Phys. Lett.* **8**, 298 (1964).
 [20] G. C. Bailey, *J. Appl. Phys.* **41**, 5232 (1970).
 [21] F. Schreiber and Z. Frait, *Phys. Rev. B* **54**, 6473 (1996).
 [22] P. Pincus, *Phys. Rev.* **118**, 658 (1960).
 [23] A. Ghosh, S. Auffret, U. Ebels, and W. E. Bailey, *Phys. Rev. Lett.* **109**, 127202 (2012).
 [24] H. T. Nembach, J. M. Shaw, C. T. Boone, and T. J. Silva, *Phys. Rev. Lett.* **110**, 117201 (2013).
 [25] Y. Li, Y. Lu, and W. E. Bailey, *J. Appl. Phys.* **113**, 17B506 (2013).
 [26] M. H. Seavey and P. E. Tannenwald, *Phys. Rev. Lett.* **1**, 168 (1958).
 [27] See the Supplemental Material at <http://link.aps.org/supplemental/10.1103/PhysRevLett.116.117602>, which includes Refs. [22–33].
 [28] M. Jirsa, *Phys. Status Solidi B* **113**, 679 (1982).
 [29] D. Y. Petrovykh, K. N. Altmann, H. Höchst, M. Laubscher, S. Maat, G. J. Mankey, and F. J. Himpsel, *Appl. Phys. Lett.* **73**, 3459 (1998).
 [30] A. Useinov, O. Mryasov, and J. Kosel, *J. Magn. Magn. Mater.* **324**, 2844 (2012).
 [31] W. E. Bailey, C. Cheng, R. Knut, O. Karis, S. Auffret, S. Zohar, D. Keavney, P. Warnick, J.-S. Lee, and D. A. Arena, *Nat. Commun.* **4**, 2025 (2013).
 [32] G. T. Rado and J. R. Weertman, *J. Phys. Chem. Solids* **11**, 315 (1959).
 [33] V. Kambarský, *Czech. J. Phys. B* **23**, 627 (1973).
 [34] W. S. Ament and G. T. Rado, *Phys. Rev.* **97**, 1558 (1955).
 [35] C. Scheck, L. Cheng, and W. E. Bailey, *Appl. Phys. Lett.* **88**, 252510 (2006).
 [36] M. Jirsa, *Phys. Status Solidi B* **113**, 679 (1982).
 [37] A. Kapelrud and A. Brataas, *Phys. Rev. Lett.* **111**, 097602 (2013).
 [38] O. Mosendz, J. E. Pearson, F. Y. Fradin, S. D. Bader, and A. Hoffmann, *Appl. Phys. Lett.* **96**, 022502 (2010).
 [39] K. Gilmore, Y. U. Idzerda, and M. D. Stiles, *Phys. Rev. Lett.* **99**, 027204 (2007).
 [40] S. M. Bhagat and P. Lubitz, *Phys. Rev. B* **10**, 179 (1974).
 [41] G. T. Rado, *J. Appl. Phys.* **29**, 330 (1958).
 [42] V. Korenman and R. E. Prange, *Phys. Rev. B* **6**, 2769 (1972).
 [43] B. A. Gurney, V. S. Speriosu, J.-P. Nozieres, H. Lefakis, D. R. Wilhoit, and O. U. Need, *Phys. Rev. Lett.* **71**, 4023 (1993).
 [44] R. D. McMichael, M. D. Stiles, P. J. Chen, and W. F. Egelhoff, Jr., *J. Appl. Phys.* **83**, 7037 (1998).
 [45] J. Zhang, P. M. Levy, S. F. Zhang, and V. Antropov, *Phys. Rev. Lett.* **93**, 256602 (2004).
 [46] R. F. Soohoo, *Phys. Rev.* **131**, 594 (1963).

Supplemental Material Wavenumber-dependent Gilbert damping in metallic ferromagnets

Yi Li and W. E. Bailey¹

*Dept. of Applied Physics & Applied Mathematics, Columbia University,
New York NY 10027, USA*

(Dated: 5 March 2016)

A. $\mu_0\Delta H_{1/2}$ for Py, uniform modes and 1st SWR modes.

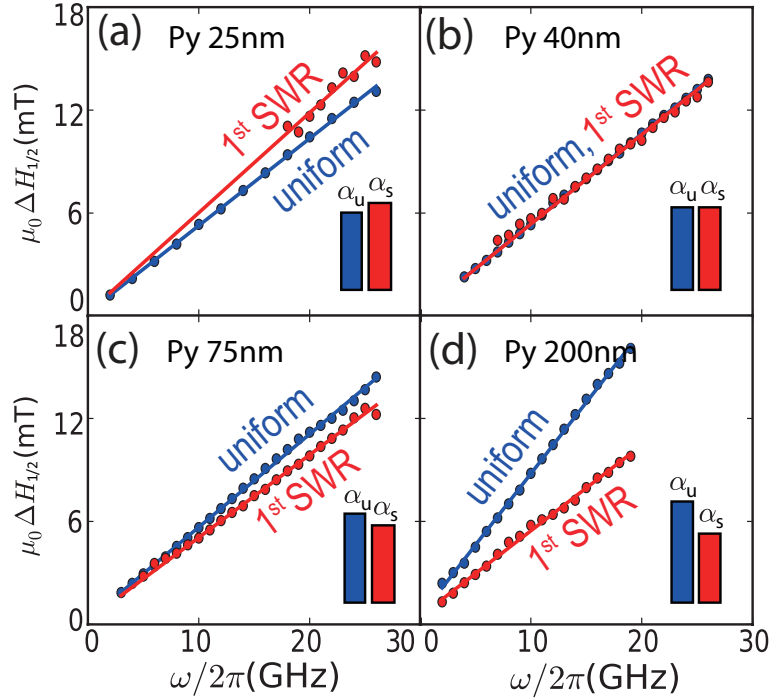


FIG. 1. Linewidths $\mu_0\Delta H_{1/2}$ for Py (a) 25 nm, (b) 40 nm, (c) 75 nm and (d) 200 nm. Lines are linear fits to the data.

B. Inhomogeneous broadening for α_u and α_s

The Gilbert damping coefficients α_u and α_s were extracted through $\mu_0\Delta H_{1/2} = \mu_0\Delta H_0 + 2\alpha\omega/\gamma$ where $\mu_0\Delta H_0$ is the inhomogeneous broadening. In the uniform modes, taking α and $\mu_0\Delta H_0$ as fitting parameters yields an average $\mu_0\Delta H_0 = 0.4, 0.1$ and 0.2 mT for Py, Co and CoFeB, respectively. The small inhomogeneous broadenings are consistent with negligible large-scale lateral inhomogeneities in the films. In the 1st SWR modes, the lowest frequency attainable is close to $\gamma\mu_0 H_{ex}/2\pi$ and proportional to $1/t_{FM}^2$. The frequency range which can be used to fit linewidths is thus restricted. In this situation we fix $\mu_0\Delta H_0$ to the values extracted from the corresponding uniform modes for $t_{FM} < 40$ nm. However we note that there may be a k^2 -dependent inhomogeneous linewidth broadening due to the inhomogeneous thickness distribution^{1,2}, in the form of:

$$\mu_0\Delta H_0 = \frac{2A}{M_s} \left(\frac{p\pi}{t_{FM}} \right)^2 \frac{2\delta t_{FM}}{t_{FM}} \quad (1)$$

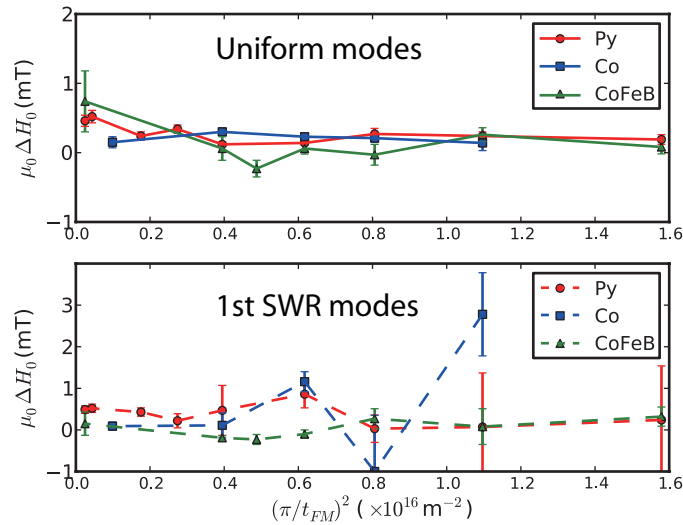


FIG. 2. Inhomogeneous linewidth as a function of $(\pi/t_{FM})^2$ extracted from the uniform modes (a) and the 1st SWR modes (b).

where p is the mode number and δt_{FM} depicts the thickness variation from surface roughness. If there is a significant roughness-lead inhomogeneous broadening, the Gilbert damping α_s could be overestimated.

Here we can exclude this mechanism by plotting the free-fitted $\mu_0 \Delta H_0$ as a function of $(\pi/t_{FM})^2$ for both uniform modes and 1st SWR modes in Fig. 2. We find no $1/t_{FM}^2$ dependence (fixed $\delta t_{FM}/t_{FM}$) or $1/t_{FM}^3$ dependence (fixed δt). The larger fluctuation of $\mu_0 \Delta H_0$ in the 1st SWR mode for Co, compared with Py and CoFeB, is due to its larger exchange splitting $\mu_0 H_{ex}$ and thus smaller frequency range to fit $\mu_0 \Delta H_0$. Thus the influence of surface roughness to the linewidth of the 1st SWR modes is negligible. We note that for higher-order SWR modes in Py 150 nm this is not the case.

C. Eddy current damping of spin wave resonance

Here we show the derivation of eddy-current damping enhancement by applying the analytical equations in Ref.³. For $p = 0$ (uniform) mode, we use Eq. (7) of Ref.³ in cgs unit

to express the even mode peak-to-peak linewidth:

$$\Delta H_p = \frac{2}{\sqrt{3}} \left[\frac{\alpha\omega}{\gamma} + \frac{2M_s d^2}{\mu_0 \delta^2 y_p^2} \left(1 - \frac{2\beta}{y_p^2 + \beta + \beta^2} \right) \right] \quad (2)$$

where α is the Gilbert damping, ω is the angular frequency, γ is the gyromagnetic ratio, M_s is the magnetization, $d = t_{FM}/2$ is the half thickness, $\delta = c/\sqrt{2\pi\sigma_c\omega}$ is the skin depth. $\beta = K_s d/A_{ex}$ characterizes the strength of surface pinning and $y_p = k_p d$ satisfies the boundary condition $y_p - \beta \cot y_p = 0$. In the limit of weak surface pinning, $\beta \sim 0$ and $y_p^2 \sim \beta - \beta^2/3$. One can obtain $\frac{1}{y_p^2} \left(1 - \frac{2\beta}{y_p^2 + \beta + \beta^2} \right) \sim 1/3$. Thus Eq. (2) becomes:

$$\Delta H_{p=0} = \frac{2\omega}{\sqrt{3}\gamma} \left(\alpha + \frac{4\pi M_s \gamma t_{FM}^2}{12\mu_0 c^2 \rho_c} \right) \quad (3)$$

Here $\rho_c = 1/\sigma_c$ is the electrical resistivity. In SI unit we find the additional damping to be:

$$\alpha_{E0} = \frac{\mu_0^2 \gamma M_s t_{FM}^2}{12\rho_c} \quad (4)$$

which we have used in the manuscript.

For $p = 1$ mode, we apply Eq. (8) of Ref.³ for the odd modes:

$$\Delta H_p = \frac{2}{\sqrt{3}} \left[\frac{\alpha\omega}{\gamma} + \frac{2M_s d^2}{\mu_0 \delta^2 y_p^2} \left(1 - \frac{2(1+\beta)}{y_p^2 + \beta + \beta^2} \right) \right] \quad (5)$$

In this case the boundary condition is $y_p + \beta \tan y_p = 0$. As $\beta \sim 0$ we can simply take $y_p = \pi/2$ for the first spin wave mode. Doing the same mathematics, we find the SI unit eddy-current damping to be:

$$\alpha_{E1} = \frac{\mu_0^2 \gamma M_s t_{FM}^2}{\rho_c} \frac{1}{\pi^2} \left(1 - \frac{8}{\pi^2} \right) \quad (6)$$

We find $\alpha_{E1} \approx 0.23\alpha_{E1}$, which is used in the manuscript for the eddy-current damping of first spin wave modes.

For higher modes, same analysis can be applied and the results are used in the mode-dependent damping analysis in Fig. 4 of the manuscript. As mode number increases, eddy-current damping decreases $\sim 1/p^2$.

D. Effective spin mixing conductance for Co/Cu/Ta and CoFeB/Cu/Ta

The effective spin mixing conductance, $g_{FM/Cu/Ta}^{\uparrow\downarrow}$, for Co and CoFeB can be calculated by taking the results from Pt spin sink⁴ into the equation:

$$(g_{FM/Cu/Ta}^{\uparrow\downarrow})^{-1} = (g_{FM/Cu/Pt}^{\uparrow\downarrow})^{-1} + (g_{Cu/Ta}^{\uparrow\downarrow})^{-1} - (g_{Cu/Pt}^{\uparrow\downarrow})^{-1} \quad (7)$$

In ref.⁴ $g_{FM/Cu/Pt}^{\uparrow\downarrow}$ are 6.8 nm^{-1} , 7.3 nm^{-1} and 9.6 nm^{-1} for FM=Py, Co and CoFeB. We can treat $g_{Cu/Ta}^{\uparrow\downarrow}$ and $g_{Cu/Pt}^{\uparrow\downarrow}$ as constants. By taking $g_{Py/Cu/Ta}^{\uparrow\downarrow} = 2.5 \text{ nm}^{-1}$ we can calculate that $g_{FM/Cu/Ta}^{\uparrow\downarrow} = 2.4 \text{ nm}^{-2}$ and 2.6 nm^{-2} for Co and CoFeB. Their values are small and close to each other, due to the high spin resistance on the Cu/Ta interface.

E. Estimation of λ_{sr}^T from $A_k k^2$ term

The quadratic wavenumber-dependent term in Gilbert damping can be interpreted as the intralayer spin pumping, with its transverse spin conductivity expressed as⁵⁻⁷ $\sigma_{\perp} = \hbar^2 n_e \tau_{sr} / 4m^*$ where n_e is the conduction electron density, m^* is the effective mass of electrons and τ_{sr} is the transverse spin relaxation time. Here we take the strong-scattering limit because the ultra-small transverse spin relaxation lengths measured by spin pumping⁸ indicates a large value of $1/\tau_{sr}$ in ferromagnets. Using wavenumber-dependent Gilbert damping term, the transverse spin relaxation length can be calculated by $\lambda_{sr}^T = v_F \tau_{sr}$ with v_F the Fermi velocity. In the calculation we use the free electron mass for m^* and $n_e = k_F^3 / 3\pi^2$ with $k_F = 1.05$, 0.96 and 1.04 \AA^{-1} for Py, Co and CoFeB^{9,10}, respectively, from the measured Fermi wave number in the majority band as an approximation. We take v_F to be 2.2×10^5 and $3.3 \times 10^5 \text{ m/s}$ for Py and Co⁹; CoFeB is assumed to take an equal v_F to that of Co. We can thus calculate that $\lambda_{sr}^T = 0.8 \text{ nm}$, 1.9 nm and 1.6 nm for Py, Co and CoFeB, respectively. Those values are in good agreement with the small transverse spin coherence lengths found in the same ferromagnetic metals^{8,11}.

F. EM+LLG Simulation Model

We have developed a model to consider eddy-current damping and spin pumping terms to the damping of spin-waves self-consistently, including the Maxwell's equations and the LLG

equation. Curves calculated using the model are shown in Figures 2 and 5 of the main text. The model is a simple extension of Rado's approach¹² for electromagnetic wave absorption in conductive ferromagnets, adapted for thin (rather than semi-infinite) films under single-sided excitation. Previously, we have applied a similar model to magnetic field distributions in magnetic heterostructures, as described in Ref¹³, *Supplemental Information*.

For the purposes of this manuscript, we have added two new terms describing intralayer and interlayer spin pumping to the LLG equation. These two novel terms are given in Eqs 18 and 33, respectively. Also, where we considered heterostructures with in-plane magnetization in Ref¹³, here we consider the simpler case of single ferromagnetic layers with film-normal magnetization, the better to isolate novel damping terms. All discussion is given in SI units to be consistent with our presentation of experiments.

Geometry: As in Refs^{12,13}, we consider a one-dimensional problem. The film plane is taken as xy , the microwave propagation direction is taken along the film thickness, $\mathbf{k} = k \hat{\mathbf{z}}$, with the sample surfaces at $z = \pm t_F/2$, where t_F is the ferromagnetic layer thickness. We define the half-thickness as $d \equiv t_F/2$. Microwaves are assumed to be incident from free space at $z = +t_F/2$; only a transmitted wave will be present at $z < -t_F/2$. The normal magnetization case is simpler than the in-plane magnetization case, as precession can be circular rather than elliptical. The film is uniformly magnetized along z with the bias field H_B applied normal to the film plane, along z . For simplicity, we assume a right-hand circularly polarized microwave field, amplitude H_0 , incident on the film, and seek right-hand circularly polarized dynamic solutions of magnetization, complex amplitude \widetilde{m}_0 :

$$\mathbf{H} = H_B \hat{\mathbf{z}} + \mathbf{H}_{\text{rf}} \quad \mathbf{H}_{\text{rf}}(z \geq t_F/2) = H_0 (\hat{\mathbf{x}} - i\hat{\mathbf{y}}) e^{i(-kz - \omega t)} \quad (8)$$

$$\mathbf{m} \simeq \hat{\mathbf{z}} + m_0 (\hat{\mathbf{x}} - i\hat{\mathbf{y}}) e^{i(-kz - \omega t)} \quad (9)$$

Characteristic lengths: Following Rado¹², we introduce the exchange length δ_{ex} and non-magnetic skin depth δ_0 , given in terms of the exchange stiffness A , magnetization M_s , conductivity σ , and RF circular frequency ω as

$$\delta_{ex} = \sqrt{\frac{2A}{\mu_0 M_s^2}} \quad \delta_0 = \sqrt{\frac{2}{\mu_0 \sigma \omega}} \quad (10)$$

in SI units, and the dimensionless values

$$\kappa \equiv \delta_{ex}k \quad 2i\epsilon^2 = 2i\frac{\delta_{ex}^2}{\delta_0^2} \quad (11)$$

for the wavenumber and the role of conductivity, respectively. The microwave frequency ω is also given in dimensionless form,

$$\Omega \equiv \frac{\omega}{\omega_M} \quad \omega_M \equiv \mu_0 M_s \gamma \quad (12)$$

where γ is the gyromagnetic ratio.

Permeability from Maxwell's equations: As Rado showed, Maxwell's equations place the following restriction on the complex susceptibility for perpendicular magnetization, $\tilde{\chi}_\perp$

$$\tilde{\chi} = \frac{\tilde{\kappa}^2 - 2i\epsilon^2}{2i\epsilon^2} \quad (13)$$

which can be found by taking the curl of the displacement-current free approximate form valid for metals

$$\nabla \times \mathbf{H} = \sigma \mathbf{E} \quad (14)$$

This expression assumes entirely local conductivity, with current $\mathbf{J}(z)$ proportional to electric field $\mathbf{E}(z)$ at each point z , a simplifying assumption neglecting nonlocal aspects of electrical conductivity in thin films. The expression is combined with the electric field expression,

$$\nabla \times \mathbf{E} = -\mu_0(1 + \chi)(\partial \mathbf{H} / \partial t) \quad (15)$$

with plane-wave solutions as specified above. The wavenumber admits complex solutions to satisfy equation 13.

Permeability from the LLG equation: At the same time, the LLG equation for magnetization dynamics, including the novel term from intralayer spin pumping,

$$\dot{\mathbf{m}} = -\mu_0 \gamma \mathbf{m} \times \mathbf{H}_{eff} + \alpha_0 \mathbf{m} \times \dot{\mathbf{m}} + A_k \mathbf{m} \times \nabla^2 \mathbf{m} \quad (16)$$

with variables as defined in the main text, can be solved substituting Eqs 8,9 for periodic motion and perpendicular magnetization in *nc*-FMR, taking $\chi = M_s m_0 / H_0$ as

$$\tilde{\chi} = \frac{1}{h_{eff} - \Omega} \quad h_{eff} = \eta + \tilde{q}\kappa^2 \quad \eta \equiv h_B - i\alpha_0\Omega - 1 \quad (17)$$

with the effect of the novel wavenumber-dependent damping term is contained in the parameter

$$\tilde{q} \equiv 1 - iA_k\delta_{ex}^{-2}\Omega \quad (18)$$

as an imaginary-valued effective field counterpart to the real-valued effective field from exchange. Here the reduced variable h in h_{eff} represents the effective field acting along the static magnetization direction normalized to the magnetization, $h \equiv H/M_s$. The frequency-dependent, imaginary effective fields show the relation $\alpha = \alpha_0 + A_k k^2$ outlined in the main text.

Dispersion relation: After equating Eqs 13 and 17 for the permeability, the electromagnetic- and spin-wave dispersion relation for κ is a biquadratic formula

$$\kappa^4 + B'\kappa^2 + C' = 0 \quad (19)$$

The coefficients B, C , are

$$B' = \tilde{q}^{-1}(\eta - \Omega) - 2i\epsilon^2 \quad C' = -2i\epsilon^2\tilde{q}^{-1}(1 + \eta - \Omega) \quad \tilde{q} \equiv 1 - iA_k\delta_{ex}^{-2}\Omega \quad (20)$$

Following Jirsa's notation³, the wavenumbers can be reduced through the half-thickness, as $y = kd$, and the dispersion relation in Eq 19 can be written equivalently as

$$y^4 - B y^2 + C = 0 \quad (21)$$

where

$$B \equiv -\Sigma B' \quad C \equiv \Sigma^2 C' \quad \Sigma \equiv \frac{d^2}{\delta_{ex}^2} \quad (22)$$

For a given frequency ω and magnetic bias field H_B , the equation can be solved through the quadratic formula, and two independent eigenmodes $\pm y_0, \pm y_1$ will exist. The amplitudes of the two different modes which can be excited are determined through boundary conditions, both for electromagnetic continuity and for surface torque on magnetization.

Field amplitudes: The auxiliary magnetic fields are expanded in the modes k_0 and k_1 through

$$H(z, t) = [a_0 \cos k_0 z + b_0 \sin k_0 z + a_1 \cos k_1 z + b_1 \sin k_1 z] (\cos \omega t \hat{\mathbf{x}} + \sin \omega t \hat{\mathbf{y}}) \quad (23)$$

with reduced magnetization amplitudes

$$m(z, t) = M_s^{-1} [\chi_0 (a_0 \cos k_0 z + b_0 \sin k_0 z) + \chi_1 (a_1 \cos k_1 z + b_1 \sin k_1 z)] (\cos \omega t \hat{\mathbf{x}} + \sin \omega t \hat{\mathbf{y}}) \quad (24)$$

where χ_i is found by substitution of k_i , determined through the quadratic formula 21, into Equation 17. The electric field amplitude is determined from Equation 14, $E_i = (\mu_0 \sigma)^{-1} (\partial/\partial z) \hat{\mathbf{z}} \times \mathbf{H}(z, t)$.

$$E(z, t) = \mu_0 \sigma [k_0 (-a_0 \sin k_0 z + b_0 \cos k_0 z) + k_1 (-a_1 \sin k_1 z + b_1 \cos k_1 z)] (-\sin \omega t \hat{\mathbf{x}} + \cos \omega t \hat{\mathbf{y}}) \quad (25)$$

Surface torques, including interlayer spin pumping: Surface anisotropy¹⁴ determines the boundary condition for the spin wave profile in the film. The transverse magnetization component \mathbf{m}_T (along x, y) is set by equating upper and lower torques on the surface magnetization, through

$$\frac{\partial m_i}{\partial z}(\pm d) \pm \frac{\widetilde{K}_s}{A_{ex}} m_i(\pm d) = 0 \quad (26)$$

where $i = x, y$ give the same surface pinning conditions for both transverse magnetization components in nc-FMR, and the same for circular polarization $m_0 = m_x - im_y$. In the absence of surface anisotropy, with $\widetilde{K}_s = 0$, y_p is entirely geometrical, with $y_p = p\pi/2$, $p = 0, 1, 2 \dots$, and $p = 0$ is the uniform mode resonance.

We assume symmetric pinning: that the surface anisotropy constant, \widetilde{K}_s , is the same at the top ($z = d$) and bottom surfaces ($z = -d$), appropriate for our nominally symmetric heterostructures. Odd- ($h \sim \sin kz$) and even- ($h \sim \cos kz$) mode resonances are given by^{3,15}

$$\widetilde{y}_p + \widetilde{\beta} \tan \widetilde{y}_p = 0 \quad (\text{odd}) \quad (27)$$

$$\widetilde{y}_p - \widetilde{\beta} \cot \widetilde{y}_p = 0 \quad (\text{even}) \quad (28)$$

where $\widetilde{\beta}$ is the pinning parameter, defined after Jirsa as³

$$\widetilde{\beta} \equiv \frac{\widetilde{K}_s d}{A_{ex}} \quad (29)$$

For uniform modes ($y \ll 1$), the resonant wavenumber due to surface anisotropy is, from Eq 28,

$$y_{r,0}^2 \simeq \beta \quad (y \rightarrow 0) \quad (30)$$

We introduce dissipation (damping) localized to the surfaces, phenomenologically, through an imaginary surface anisotropy energy¹⁶

$$\widetilde{K}_s = K'_s + iK''_s \quad (31)$$

making β and $y_{r,0}$ complex. This term can represent surface-related damping α_{surf} of any type as long as the torque it exerts on magnetization is localized to the surface; the effect would include conventional (interlayer) spin pumping and possibly resistivity-type damping from surface scattering. The effect of the complex surface anisotropy on damping can be seen through the dispersion relation in Eq 21: in the limit of small conductivity, $\delta_0 \rightarrow \infty$ and $2i\epsilon^2 \rightarrow 0$, Eq 21 becomes $y^2 \simeq -B$, and $\text{Im}(y^2) = \alpha_0 \Omega \Sigma$. Equating $\text{Im}(y^2) = \alpha \Omega \Sigma$ and $\text{Im}(y_{r,0}^2) = K''_s d/A$ yields $K''_s = \alpha \omega M_s d / (2\gamma)$. To represent spin pumping, we equate the surface-related damping α_{surf} to the spin pumping term

$$\alpha^{surf} = 2 \frac{|\gamma| \hbar g_r^{\uparrow\downarrow}}{4\pi M_s t_F} \quad (32)$$

in SI units, where the factor of two represents the effect from both top and bottom surfaces (symmetric pinning) and $g_r^{\uparrow\downarrow}/S$ is the spin mixing conductance in units of m^{-2} .

$$K''_s = \frac{g_r^{\uparrow\downarrow}}{S} \left(\frac{\hbar \omega}{8\pi} \right) \quad (33)$$

Boundary conditions and solution: Through the relations presented to this point, there are six boundary conditions for the conductive magnetic thin film: surface torques, E-field continuity, and H-field continuity, all at both top and bottom surfaces. There are eight

unknown coefficients: reflected and transmitted $E_{r,t}$ and $H_{r,t}$ amplitudes for the monochromatic microwaves in free-space at the two surfaces, and the four values of a_i , b_i pertaining to the H -field distributions inside the film given in Eq 23. The 8×6 system of equations can be reduced to a 4×2 system, represented through a transfer matrix \mathbf{M} , $[E_d, Hd]^T = \mathbf{M} [E_{-d}, H-d]^T$). In the case of the single layer, incident, reflected, and transmitted waves can be written in terms of the H -field only, with $E = \pm\mu_0cH$, making all field distributions soluble in terms of the incident H -field.

For unit incident fields, absorbed power is calculated through the Poynting theorem. We fit Lorentzian curves to the absorption in the vicinity of the SWR, and extract values of damping α from the linewidth. Calculated linewidths match the analytical approximate calculations for eddy-current linewidth under finite surface anisotropy presented in Ref³, for the absence of novel torques, to 5% or better. We have verified numerically that all linewidths are Gilbert type in the model; this can be seen immediately through the effective fields in Eq 17, with all imaginary effective-field terms proportional to frequency Ω .

REFERENCES

- ¹G. C. Bailey, *J. Appl. Phys.* **41**, 5232 (1970).
- ²F. Schreiber and Z. Frait, *Phys. Rev. B* **54**, 6473 (1996).
- ³M. Jirsa *phys. stat. sol. (b)* **113**, 679 (1982).
- ⁴A. Ghosh, J. F. Sierra, S. Auffret, U. Ebels and W. E. Bailey, *Appl. Phys. Lett.* **98**, 052508 (2011).
- ⁵E. M. Hankiewicz, G. Vignale and Y. Tserkovnyak, *Phys. Rev. B* **78**, 020404(R) (2008).
- ⁶Y. Tserkovnyak, E. M. Hankiewicz and G. Vignale, *Phys. Rev. B* **79**, 094415 (2009).
- ⁷H. T. Nembach, J. M. Shaw, C. T. Boone and T. J. Silva, *Phys. Rev. Lett* **110**, 117201 (2013).
- ⁸A. Ghosh, S. Auffret, U. Ebels and W. E. Bailey, *Phys. Rev. Lett* **109**, 127202 (2012).
- ⁹D. Y. Petrovykh, K. N. Altmann, H. Höchst, M. Laubscher, S. Maat, G. J. Mankey and F. J. Himpsel, *Appl. Phys. Lett.* **73**, 3459 (1998).
- ¹⁰A. Useinov, O. Mryasov and J. Kosel, *J. Magn. Magn. Mater.* **324**, 2844 (2012).
- ¹¹J. Zhang, P. M. Levy, S. F. Zhang and V. Antropov, *Phys. Rev. Lett.* **93**, 256602 (2004).
- ¹²W. S. Ament and G. T. Rado, *Phys. Rev.* **97**, 1558 (1955).

- ¹³W. E. Bailey, C. Cheng, R. Knut, O. Karis, S. Auffret, S. Zohar, D. Keavney, P. Warnick, J.-S. Lee and D. A. Arena, *Nature Comm.* **4**, 2025 (2013).
- ¹⁴G. T. Rado and J. R. Weertman *J. Phys. Chem. Solids* **11**, 315 (1959).
- ¹⁵R. F. Soohoo, *Phys. Rev.* **131**, 54 (1963).
- ¹⁶V. Kamberský, *Czech. J. Phys. B* **23**, 627 (1973).